Photophysical Properties of Structurally and Electronically Modified Flavin Derivatives Determined by Spectroscopy and Theoretical Calculations

Susanne Salzmann,[†] Víctor Martinez-Junza,[‡] Björn Zorn,[‡] Silvia E. Braslavsky,[‡] Madina Mansurova,[‡] Christel M. Marian,*[,†] and Wolfgang Gärtner*[,‡]

Institute of Theoretical and Computational Chemistry, Heinrich Heine University, Düsseldorf, Universitätsstrasse 1, Geb. 26.32, 40225 Düsseldorf, Germany, and Max-Planck-Institute for Bioinorganic Chemistry, Postfach 101365, 45410 Mülheim an der Ruhr, Germany

Received: June 18, 2009; Revised Manuscript Received: June 25, 2009

Four different riboflavin (RF) derivatives, two electronically modified compounds (1- and 5-deazariboflavin, 1DRF and 5DRF) and two sterically modified compounds (7,8-didemethyl- and 8-isopropylriboflavin, DMRF and *ipr*RF), were subjected to a combination of time-resolved measurements (absorption and fluorescence) and high-level quantum chemical investigations. Both alkyl-modified flavins showed similar fluorescence properties as the parent compound, yet 5DRF had a larger quantum yield of fluorescence ($\Phi_F = 0.52$) than RF ($\Phi_F = 0.27$). Interestingly, 1DRF did not show fluorescence at all under these steady state conditions. The triplet quantum yield was different for the modified flavins such that no triplet formation was found for 1DRF, whereas the other compounds all formed triplet states (Φ_{TR} for 5DRF of 0.64 and 0.50 and 0.23 for *ipr*RF and DMRF, respectively). The triplet states of the two alkyl-modified flavins decayed with similar time constants as the parent compound, whereas a shorter lifetime was measured for 5DRF ($\tau_{TR} = 15$ μs, compared to $\tau_{TR} = 29$ μs for RF). In the calculations, the flavin derivatives were modeled as lumiflavins, that is, without the ribityl chain. We conclude that for aqueous solutions of DMRF, *ipr*RF, and 5DRF intersystem crossing (ISC) takes place from the S_1 $^1(\pi\pi^*)$ to the T_2 $^3(\pi\pi^*)$ state by a vibronic spin−orbit coupling mechanism, a process common to most flavins, whereas ISC is slow in excited 1DRF due to the absence of a close-by triplet state.

Introduction

Flavins are widely found in nature as cofactors of many enzymes in which their versatile redox properties make them available for various roles.[1] In addition, there is an increasing interest in their photochemical properties since their discovery as chromophores in blue-light sensing photoreceptors.[2] Different light-induced reaction pathways of flavins (riboflavin RF, flavin mononucleotide FMN, and flavin adenine nucleotide FAD, Figure 1) in the various photosensory pigments have been detected (covalent bond formation, stable radical formation, hydrogen bond rearrangements, and electron transfer reactions)[3] and, in fact, many research activities of both experimental and theoretical groups have been triggered by these discoveries.[4−21] However, in order to unravel those light-induced reactions (e.g., the formation of the reactive triplet species of FMN in the light, oxygen, and voltage (LOV) domains of phototropin), a detailed knowledge of the electronic structure as well as the competing dissipation mechanisms is of particular importance.

We recently reported the improved chemical synthesis of two deaza-compounds (1- and 5-deazariboflavin, 1DRF and 5DRF) and two sterically modified compounds (7,8-didemethyl- and 8-isopropylriboflavin, DMRF and *ipr*RF; for modifications, see Figure 1) in combination with the determination of their first absorption maxima and midpoint potentials.[22] With respect to their potential role as cofactors in photosensitive pigments, the energy dissipation processes of these flavin derivatives are of utter interest. We already could demonstrate that triplet generation in flavins follows different reaction mechanisms in gas phase and in solution.[9] With a combination of experiment and theory, the spectroscopic properties of these compounds are investigated in this report. Hereby, we take a special interest in the mechanism of the triplet state generation.

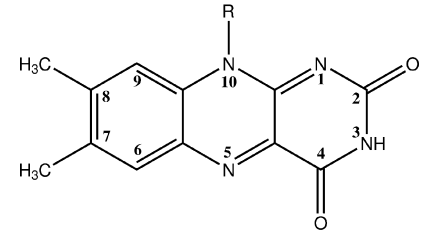

Figure 1. Chemical structure and labeling of flavins. R = CH_3, lumiflavin; R = ribityl, riboflavin; R = ribityl-5′-phosphate, FMN, flavin mononucleotide; R = ribityl-(9-adenosyl)-pyrophosphate, FAD, flavin adenine dinucleotide.

Experimental and Computational Details

Experimental Setup. The chemical synthesis and electrochemical properties of the flavin derivatives investigated here have recently been reported.[22] Fluorescence spectra of the water solutions of the flavin derivatives were recorded with a Cary Eclipse spectrometer (Varian, Palo Alto, USA) at an absorbance of $A = 0.145$ (DMRF, *ipr*RF), and of $A = 0.0775$ (5DRF) at their respective absorption maximum. The same solutions were used for determination of the fluorescence lifetimes in a FL920 spectrometer (Edinburgh Instruments, UK). Triplet quantum

* To whom correspondence should be addressed. E-mail: (C.M.M) Christel.Marian@uni-duesseldorf.de; (W.G.) gaertner@mpi-muelheim.mpg.de.
[†] Heinrich Heine University.
[‡] Max-Planck-Institute for Bioinorganic Chemistry.

10.1021/jp905724b CCC: $40.75
Published on Web 07/29/2009

yields Φ_{Tr} of the flavin derivatives were determined by comparison to the known triplet quantum yield of RF. For the latter, the literature value of $\Phi_{Tr} = 0.6$ was used as reference.[37]

Transient absorbance changes after nanosecond-laser flash excitation were recorded using a LFP111 from Luzchem, Ontario, Canada. Excitation was from a Nd:YAG driven tunable OPO laser (Nd:YAG, Innolas, Garching, Germany; OPO, GWU Lasertechnik, Erftstadt, Germany). The experiments were performed in the linear laser energy dependence region of the transient absorbance changes. The flavin derivatives were dissolved in tridistilled water ($A = 0.2$), and the solutions were bubbled with nitrogen for 30 min prior to use. Samples were excited at $\lambda = 422$ nm (5DRF) and at $\lambda = 432$ nm (DMRF and *ipr*RF). For both wavelengths, a riboflavin sample with matching absorbance was used as reference. Data analysis was performed with the Origin software.

Computational Details. For the details of the geometry optimizations and the calculation of harmonic vibrational frequencies ((TD)DFT/TZVP) as well as the determination of excitation energies, dipole moments, and oscillator strengths of dipole-allowed transitions (DFT/MRCI/TZVP) we refer to earlier work.[9]

Theoretical radiative decay rates were obtained according to eq 1

$$k_{rad} = \frac{4e^2}{3c^3\hbar^4}(E_i - E_f)^3|\langle f|\vec{r}|i\rangle|^2 \qquad (1)$$

Expressing k_{rad} in units of s^{-1}, ΔE in cm^{-1} and $\mu_{el} = \langle f|\vec{r}|i\rangle$ in atomic units (ea_0), the numerical prefactor becomes 2.0261×10^{-6}. If $|i\rangle$ is chosen to be the wave function of the S_1 state, here determined at the DFT/MRCI level, and $\langle f|$ is the corresponding ground state wave function, then k_{rad} represents the fluorescence rate k_F of the compound. Equation 1 can also be used to evaluate the rates of spin-forbidden radiative transitions. In this case, spin−orbit mixed wave functions of the initial and final states, obtained here via MRSOCI,[23] have to be employed. In the so-called high-temperature limit, which applies here, all fine-structure sublevels of the T_1 state are populated equally and their individual transition rates have to be averaged to yield the phosphorescence rate k_P.

Intensity distributions of the vibronic absorption transitions were determined using in the Franck-Condon (FC) approximation with the VIBES program developed in our laboratory.[24] Attending to efficiency reasons, not all modes were included. After careful testing, 30 modes with the largest displacements in the Duschinsky transformation were selected. For better comparison with the experimental data, the line spectra were broadened by Gaussian functions with constant full width at half-maximum (fwhm) of 1000 cm^{-1}.

In the Condon approximation, electronic spin−orbit coupling matrix elements and vibrational overlaps are required for the theoretical determination of ISC rates. SOMES between the correlated DFT/MRCI wave functions were calculated using the SPOCK program developed in our laboratory.[25,26] The one-center mean-field approximation to the Breit−Pauli Hamiltonian was used for the description of the spin−orbit coupling for reasons of efficiency. This nonempirical effective one-electron operator treats the expensive two-electron terms of the full Hamiltonian in a Fock-like manner[27,28] and has been shown to yield an accuracy better than 5% of the full treatment.[29,30] Vibrational overlaps were determined employing the VIBES program.[24] Recent studies had shown, however, that a proper description of the nonradiative decay of the S_1 state of flavins in aqueous solution requires going beyond the Condon approximation.[9] To that end, the derivatives of the SOMES, necessary for evaluating the Herzberg−Teller type expansion of spin−orbit coupling around the $^1(\pi\pi)^*$ state minimum to first order, were calculated numerically by finite difference techniques as described.[31] Rate constants for the nonradiative decay of the S_1 state caused by vibronic spin−orbit coupling were also calculated using the VIBES program.[24] Herein, all totally symmetric and all out-of-plane (oop) vibrational modes were used as accepting and coupling modes, respectively. For more detailed information on the entities required for the evaluation of the ISC rate constants see the Supporting Information.

To estimate spectral shifts due to electrostatic interaction in polar solvents, we employed the COSMO which is implemented in the TURBOMOLE package.[32] The relative static permittivity (formerly called dielectric constant) of water at ambient temperature, $\varepsilon = 78$, was used. Due to technical reasons, C_1 symmetry had to be used for all calculations involving COSMO. For both singlet and triplet multiplicity 20 roots were computed. Since COSMO is not able to model hydrogen bonding, the effects of hydrogen bonding were mimicked by microhydration with four explicit water molecules as described in previous work.[9] UDFT was employed for the optimization of the first triplet state of this complex.

TABLE 1: Spectroscopic Properties of Four Structurally Modified Riboflavins and of the Parent Compound (RF)

	λ_{abs} (max)[a]/nm	ε_{max}[a]/M^{-1} cm^{-1}	λ_{em} (max)/nm	τ_{Fl}/ns	Φ_{Fl}
RF	450	12460	520	4.8	0.27
1DRF	537	6800	n.d.[b]	n.d.[b]	n.d.[b]
5DRF	400	12460	441	5.0	0.52
DMRF	436	12460	520	3.9	0.27
*ipr*RF	448	12460	520	4.7	0.27

[a] Taken from ref 22, Table 1. [b] For a detailed investigation of the fluorescence properties of 1DRF, see ref 34.

Results and Discussion

Absorption and Fluorescence Properties of Modified Flavins. Four RF derivatives were studied, 1DRF and 5DRF, showing an electronically modified structure, and the two sterically modified compounds, DMRF and *ipr*RF (for changes with respect to the structure of the parent compound, see Figure 1). The modifications cause altered absorption maxima and molar absorption coefficients, as compared to riboflavin, in particular in the two deaza derivatives (Table 1). 1DRF showed a strong bathochromic shift of its absorption maximum ($\lambda_{max} = 537$ nm) and a reduced molar absorption coefficient ($\varepsilon_{max} = 6800$ M^{-1} cm^{-1}), and the 5-deaza derivative showed a similar molar absorption coefficient as RF, but a significant hypsochromic shift of its absorption maximum ($\lambda_{max} = 408$ nm). The demethyl compound also showed a small hypsochromic shift in its absorption maximum ($\lambda_{max} = 436$ nm), whereas the absorption maximum of *ipr*RF was practically identical to that of the parent compound. Both alkyl-modified RF compounds had absorption coefficients identical to riboflavin.

No fluorescence was detected for 1DRF by steady-state measurements, in agreement with the known literature.[33] However, experiments using subnanosecond pulses revealed a clearly detectable fluorescence for this compound in the short picosecond time range.[34] The other flavin derivatives showed a substantial fluorescence quantum yield (Table 1). Similar fluorescence quantum yields as those for riboflavin ($\Phi_F =$

TABLE 2: Properties of Flavin Triplet States; λ_{max} and λ_{min} Refer to the Transient Absorption Maximum and Minimum (Bleaching) Immediately after the ns Laser Pulse; τ_{Tr} Is the Triplet Lifetime in Aqueous Solution under the Degassing Conditions Used

	$\tau_{Tr}/\mu s$	λ_{max}/nm	λ_{min}/nm	Φ_{Tr}
RF	29	390, 520, 700	450	0.60
1DRF[a]				
5DRF	14	500	410	0.64
DMRF	24	380, 510, 630	450	0.23
*ipr*RF	27	520, 700	460	0.50

[a] No triplet formation was observed for this compound.

0.27)[35] were determined for the demethyl derivative and for *ipr*RF ($\Phi_{Fl} = 0.27$), but a significantly larger quantum yield, $\Phi_{Fl} = 0.52$, was found for the 5-deaza compound. The fluorescence decay time of the demethyl derivative ($\tau_{Fl} = 3.9$ ns) was slightly shorter than that of RF ($\tau_{Fl} = 4.8$ ns for RF), whereas the corresponding values for 5DRF (5 ns) and for *ipr*RF (4.7 ns) were in the same range as that for the parent compound RF.

The data obtained for 5DRF can be compared to those reported by Isińska-Rak et al.[36] although their measurements for 5DRF were performed in acetonitrile and methanol, whereas we measured in water. Excellent agreement was found for RF ($\tau_{Fl} = 4.8$ versus 5.1 ns, $\Phi_{Fl} = 0.27$ versus 0.28), whereas the parameters for 5DRF determined here differ significantly from those cited above[36] ($\tau_{Fl} = 5.0$ versus 4.03 ns, and $\Phi_{Fl} = 0.52$ versus 0.11). This may be attributed to the different solvents used, but this behavior requires a more detailed comparative investigation.

Time-Resolved Absorption Changes. Nanosecond laser flash excitation of the riboflavin derivatives caused transient absorption changes, except for 1DRF, which remained practically unchanged over the whole observation time. For the other three RF derivatives the absorption band underwent transient bleaching, concomitant with the formation of broad, structured absorption bands that extended far into the long wavelength range (Table 2). Riboflavin showed the formation of a broad absorption with maxima at 520 and ca. 700 nm with a quantum yield of 0.6 that decayed with a 29 μs lifetime. One should be aware that the reported quantum yields vary significantly from 0.4 up to 0.6.[37−39] These variations reported in the literature arise from varying experimental conditions with the pH value of the solution being the most dominating factor changing the spectroscopic properties of flavins. The 5-deaza compound showed formation of a triplet band with a maximum around 500 nm (Figure 2). This species showed a slightly higher quantum yield ($\Phi_{Tr} = 0.64$) and decayed faster than RF ($\tau_{Tr} =$ 14 μs). Smaller quantum yields were determined for the two alkyl modified compounds: $\Phi_{Tr} = 0.23$ (decay time $\tau_{Tr} = 24$ μs) for DMRF, and $\Phi_{Tr} = 0.50$ (decay time $\tau_{Tr} = 27$ μs) for *ipr*RF. The formation of broad, structured transient absorption bands was detected also for these compounds (only the spectrum of 5DRF are shown here).

For 1DRF, the absence of any triplet formation under the measuring conditions concurs with recently performed fluorescence measurements on a picosecond time scale. In contrast to literature reports, these experiments revealed a biphasic fluorescence decay with ca. 2 and 12 ps.[34] Although one would not expect a triplet formation as a competing deactivation process, we cannot exclude a very low yield of triplet formation ($\Phi_{Tr} <$ 0.05) for 1DRF that would be below our detection limit. A comparison with recently reported[36] triplet parameters for 5DRF revealed again deviations; these authors measured a significantly longer triplet lifetime of 105 μs in contrast to the value of 14 μs found by us.

Calculated Electronic Absorption Spectra. It has been shown earlier that the spectroscopic properties of RF and LF are nearly identical.[40−42] For this reason, the bulky ribityl chain was substituted by a methyl group in all calculations. Accordingly, the flavin compounds RF, DMRF, 1DRF, and 5DRF were modeled by LF, DMLF (= 10-methylisoalloxazine, MIA, in ref 9), 1DLF, and 5DLF, respectively.

The ground and excited state geometries of LF and DMLF were taken from earlier work.[9] Except for the now present C−C bonds being longer than the original C−N bonds, the exchange of the nitrogen atoms at positions 1 or 5 for a CH-group showed no major effect on the nuclear structure (for more information see Supporting Information). To facilitate the discussion, the minimum nuclear arrangement of the first excited singlet state is denoted $^1(\pi\pi^*)$ and the optimized geometry of the first triplet state is labeled $^3(\pi\pi^*)$.

LF and DMLF as Models for RF and DMRF. The photophysical properties of the three flavin compounds IA, DMLF, and LF in vacuum and in solution had been the topic of earlier work.[9] Thus, only a short abstract of the calculated vertical excitation spectra of LF and DMLF is given below. For a detailed comparison and discussion of our DFT/MRCI excitation energies of all three flavin compounds with experimental data and with earlier quantum chemical investigations, see ref 9.

Flavins show usually three absorption bands in the wavelength range longer than 250 nm. In previous quantum chemical studies, they have all been assigned to ($\pi \rightarrow \pi^*$) transitions.[9−15] The first band in the absorption spectrum corresponds to a transition from the ground state to the lowest-lying excited state of the singlet manifold (S1) of LF and DMLF and is dominated by the ($\pi_H \rightarrow \pi_L^*$) (HOMO−LUMO) excitation. The position of that band is nearly unaffected by the surrounding solvent.[13,43] In contrast, the second visible band in the spectrum is known to exhibit a pronounced red shift in polar and protic solvents.[13,41,43] In the vacuum, this state corresponds to the fourth excited singlet state (S4) and is mainly dominated by the ($\pi_{H-1} \rightarrow \pi_L^*$) excitation. The most intensive of these three bands is found in the UV spectral region around 250 nm. It arises mainly from the ($\pi_H \rightarrow \pi_{L+1}^*$) excitation.[9]

Our calculations yield vertical excitation wavelengths of 432 nm for LF and 421 nm for DMLF for aqueous solution (referring to values in the gas phase of 422 and 409 nm, respectively). Although it is a common practice to identify the measured absorption maxima with vertical excitation energies, it has been shown that this approach is not always correct.[44−46] In cases when the geometry shift is small, as for all flavins presented here, the vibrational wave functions do not necessarily have their maxima at the classical turning points,[46] and a displacement of the absorption maximum from the vertical excitation energy can occur (for more information see Supporting Information). The simulated FC $S_0 \rightarrow S_1$ absorption spectra of LF and DMLF are shown in Figure 3 together with the computed vertical excitation energies and the measured spectra of RF and DMRF. It is seen that the maxima of the simulated $S_0 \rightarrow S_1$ absorption bands are significantly red shifted with respect to the vertical excitation energies. A comparison with the measured peak positions and band shapes shows good agreement.

The second band, originating from the ($\pi_{H-1} \rightarrow \pi_L^*$) excitation shows a slightly lower oscillator strength than the first bright transition. With our best solvation model (COSMO + micro-

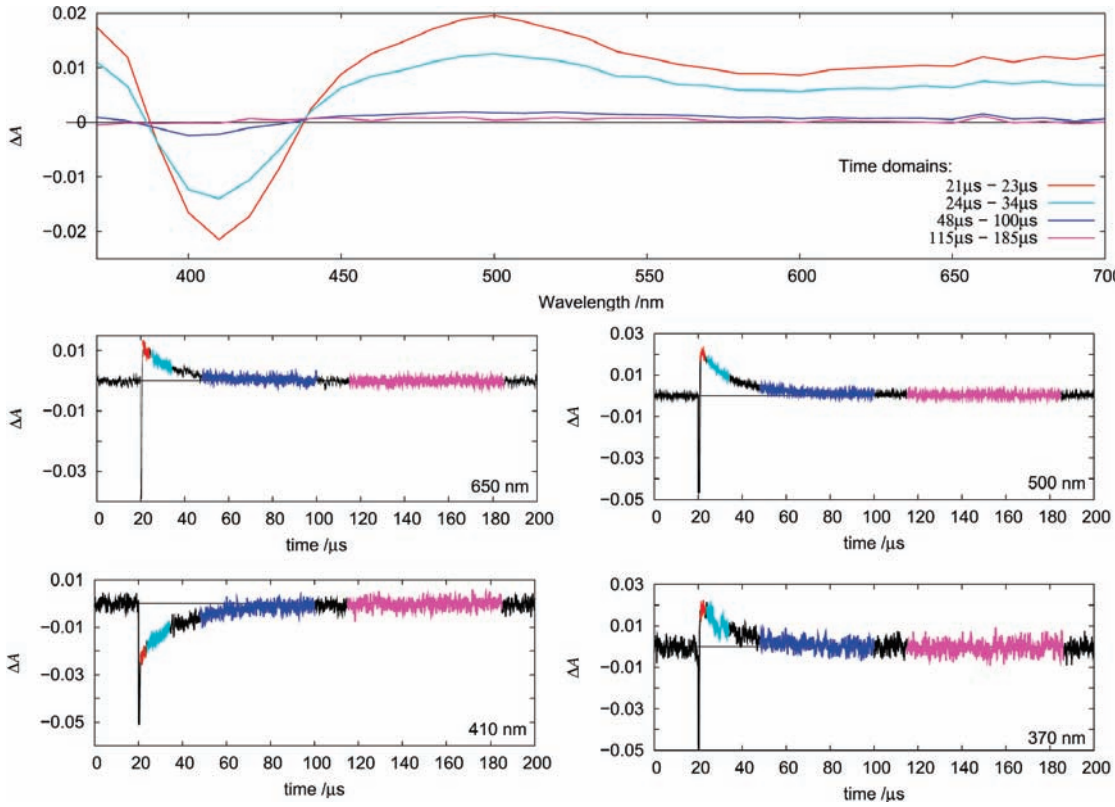

Figure 2. Transient absorption spectra of 5DRF for different time domains (uppermost panel) and kinetic traces at various wavelengths: 650, 500, 410, and 370 nm. The color coding of the kinetic traces refers to the color coding of the transient spectra.

hydration), we find a vertical excitation wavelength at 357 nm for LF and 343 nm for DMLF, respectively, in very good agreement with the measurements (375 nm for LF and 349 nm for DMLF). The energetic position of the third band is also well reproduced by the calculations. Furthermore, good qualitative agreement in the considered energy range is found between the computed and measured relative intensities of all optically bright transitions (Figure 3).

Low-lying nπ* states that are involved in the photophysics of LF and DMLF in the gas phase, do not play a major role in the low-energy regime of these flavins in aqueous solution, where these states are blue shifted by up to 0.7 eV (Table 3). This does not exclude a participation of the ^{1}(nπ*) states via vibronic coupling at elevated temperatures as described by Weigel et al.[47]

1DLF and 5DLF as Models for 1DRF and 5DRF, Respectively. The absorption spectra of both deaza derivatives, 1DLF and 5DLF, differ with respect to the parent compound such that 1DRF exhibits a strong bathochromic shift, whereas the absorption maximum of 5DRF is hypsochromically shifted (Table 1). Inspection of the optimized ground and excited state geometries reveals that structural changes are mostly restricted to the bonds adjacent to the substituted atoms (for more information see Figure S5 and S6 of the Supporting Information). Therefore, we can exclude purely geometrical effects as the origin of the altered spectroscopic properties. In order to shed some light on the spectroscopic shifts, the orbital energies of three decisive frontier π orbitals for all calculated compounds, the total energies of the two deaza flavins, 1DLF and 5DLF, and three MOs of LF are shown in Figure 4.

In a simplified picture, the excitation energies depend on the differences between the orbital energies of the orbitals involved. As can be seen in Figure 4 (left), the orbital energies of 1DLF and 5DLF differ from those of the parent compound LF, which serves as reference in the following discussion. The π_H MO (HOMO) of 1DLF is destabilized, whereas no significant energy shift is found for 5DLF. The fact that the destabilization is more pronounced for the LUMO (π_L*) of 5DLF can be rationalized as follows. The charge distribution at the N(1) and N(5) positions is very different for the two MOs π_H and π_L*. The Coulomb attraction between the electrons and the nucleus is larger at the N center than at the C center. Therefore, exchange of an iminic nitrogen atom for a CH group causes a destabilization, if substantial electron density is found at the respective center. Hence, substitution at the N(1) position, influences the π_H MO, whereas the position of the π_L* MO is nearly unaffected. This results in a red shift of the absorption. Substitution at the N(5) position, on the other hand, leads to a considerable destabilization of the π_L* MO, consequently causing a blue shift of the absorption, since the π_H MO remains widely unaffected.

The vertical excitation wavelength of the first excited singlet state of 1DLF (see Table 4) in the gas phase is red shifted by about 50 nm to 473 nm with respect to the parent compound. As in LF, this state is dominated by the $\pi_H \rightarrow \pi_L$* (HOMO−LUMO) transition. Polarity and effects of hydrogen bonding of the solvent accumulate an additional red-shift. We find a vertical excitation energy of 515 nm with our best solvent model. The band maximum in aqueous solution, as estimated from the simulated FC spectrum, is located at 553 nm, in good agreement with the experiment (537 nm for 1DRF). The position of the second optically bright band is unaffected by the replacement of the N(1) atom by a CH group. However, its oscillator strength is drastically smaller than that of LF. Similar to the parent compound, it is red shifted by almost 0.4 eV in water. According to our calculations, more than one electronic transition contributes to the third band, which exhibits a pronounced shoulder at its short-wavelength side and is the strongest band in the considered energy regime.

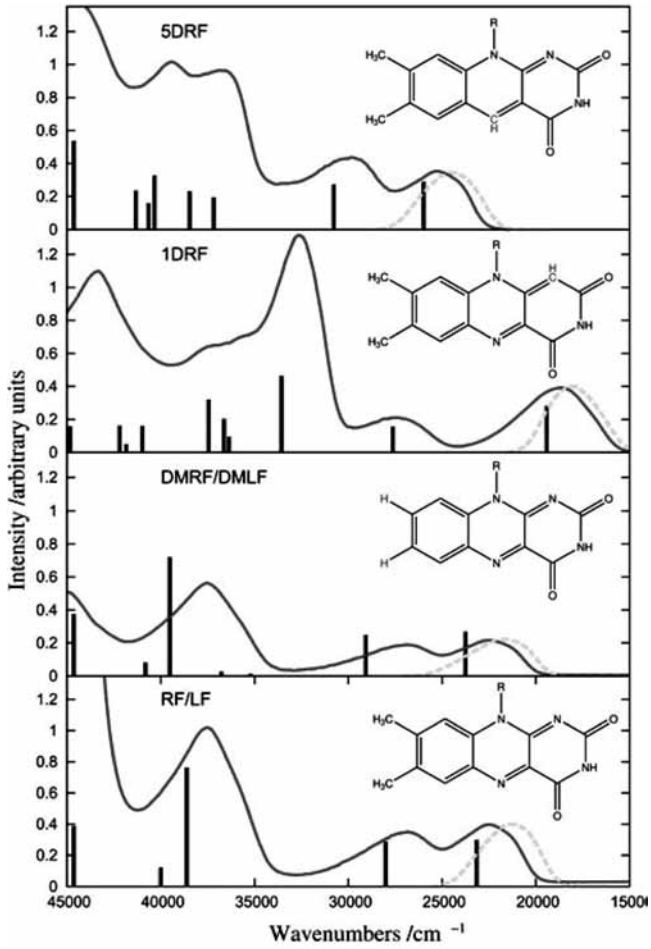

Figure 3. LF, DMLF, 1DLF and 5DLF. Comparison between experimental absorption spectra of the riboflavin derivatives (full lines) and DFT/MRCI vertical excitation energies and intensities of the lumiflavin derivatives (vertical lines) in water. In addition, simulated FC $S_0 \rightarrow S_1$ absorption bands (dashed line) are shown. For easier comparison with experiment, the computed line spectrum (not shown) was broadened by Gaussian functions with fwhm = 1000 cm^{-1}.

The energetic positions of the dark nπ^* states in 1DLF are rather unaffected by water. Because of the substantial red shift of the $^1(\pi\pi^*)$ (S1) band, the $^1(n\pi^*)$ states are located more than 0.6 eV above that band in the vacuum. In water, the energy gap is even larger than 1 eV, excluding that the $^1(n\pi^*)$ states contribute to the photophysics of the first absorption band.

The two lowest-lying absorption bands of 5DLF (see Table 5) are blue shifted with respect to those of the parent compound LF. However, unlike for 1DLF, the energetic position of the first absorption band ($\pi_H \rightarrow \pi_L^*$) (HOMO−LUMO) is not very sensitive to the environment. Whereas the vertical excitation wavelength is calculated in vacuum to be 397 nm, it is found at 385 nm in aqueous solution. The band maximum in water is estimated at 408 nm, close to the experimental value of 400 nm (Figure 3). An excitation energy of 304 nm in the gas phase and 325 nm in aqueous solution is determined for the second band. Five energetically close-lying electronic transitions with significant oscillator strengths are made responsible for the strange shape of the third absorption band in the experimental spectrum of 5DRF. Similar to the parent compounds, good qualitative agreement between the calculated and measured relative intensities of the first three absorption bands of the deaza derivatives is observed.

Even in vacuum, the experimentally not observable $^1(n \rightarrow \pi^*)$ transitions are blue-shifted by at least 0.5 eV with respect to the parent compound, in agreement with earlier TDDFT investigations of 5DRF.[36]

Calculated Fluorescence Rate Constants. Adiabatic excitation energies and radiative decay rate constants for the $^1(\pi\pi^*)$ state minimum nuclear arrangements are listed in Table 6. As found in earlier work,[9] the adiabatic excitation energies of the first $^1(\pi\pi^*)$ states of LF and DMLF are very similar. The onset of the absorption is somewhat blue shifted for the $^1(\pi\pi^*)$ state of DMLF with respect to LF, in agreement with the experimental findings.

As anticipated from the vertical excitation energies, the adiabatic excitation energies of 1DLF are red shifted with respect to the parent compound, whereas a blue shift is observed for 5DLF. Our model does not allow determining the solvent shift for emission in the same satisfying manner as for absorption. However, since the LF and DMLF transition energies show almost no solvent shifts, we expect the fluorescence rates in water to remain unchanged with respect to the gas phase.

The solvent causes a hypsochromic shift in the emission of 5DLF. Since the fluorescence rate constant is proportional to the cube of the emission energy, we expect the rate to increase in water. Concurrent with this trend, our calculated fluorescence rate constants show an excellent overall agreement with the experimental findings for RF, RMRF, and 5DRF. As pointed out above, 1DRF behaved differently and showed a fluorescence decay in the picoseconds time range.[34]

Triplet Generation. As already stated in the Introduction, the light-induced reactions in the flavin-binding, blue-light photosensors comprise different reaction mechanisms of the flavin chromophores. The signaling reactions range from covalent bond formation (via a reactive triplet transient) to stable radical formation, hydrogen bond rearrangements, and electron transfer reactions. Clearly, the dissipation mechanisms that depopulate the primarily excited singlet state of the flavin cofactor strongly depend on the environmental surroundings.

In all flavin derivatives studied in this work, the lowest-lying excited triplet state (T_1) is dominated by the $\pi_H \rightarrow \pi_L^*$ (HOMO−LUMO) transition. In LF and DMLF, its energetic position is mostly solvent independent. For the ordering of the second and third excited triplet states, which are energetically close to the S_1 state, the environment plays a decisive role. In the vacuum, the $^3(n\pi^*)$ state is situated below S_1 and the second $^3(\pi\pi^*)$ state is situated above (see Table 3). This order reverses in aqueous solution, which is momentous for the ISC mechanism (see below). Similar to the singlet case, the lowest-lying excited triplet state of 1DLF is red shifted by solvent effects (see Table 4). Contrary to LF, there is no second triplet state situated below the S_1 state in the vertical spectrum of 1DLF, neither in the vacuum nor in solution. Hence, only the T_1 state can contribute to the depopulation of the S_1 state via ISC. Considering 5DLF, the first excited triplet state in the FC region shows a similar blue shift as its singlet counterpart. In the vacuum there is no other triplet state found below the S_1 state. However, the second $^3(\pi\pi^*)$ state is energetically close. In aqueous solution, this state is located below the S_1 state and possibly participates in the energy dissipation of that state (see Table 5).

In previous work, we have shown that due to the above-mentioned sensitivity of several low-lying excited triplet states to the environment, the triplet generation in flavins follows different mechanisms for gas phase and aqueous solutions.[9] Back then, due to efficiency reasons the ISC rate constants were only calculated for the smallest compound (IA in ref 9), because the number and the frequencies of the normal modes are of importance for the computational expense of the vibrational

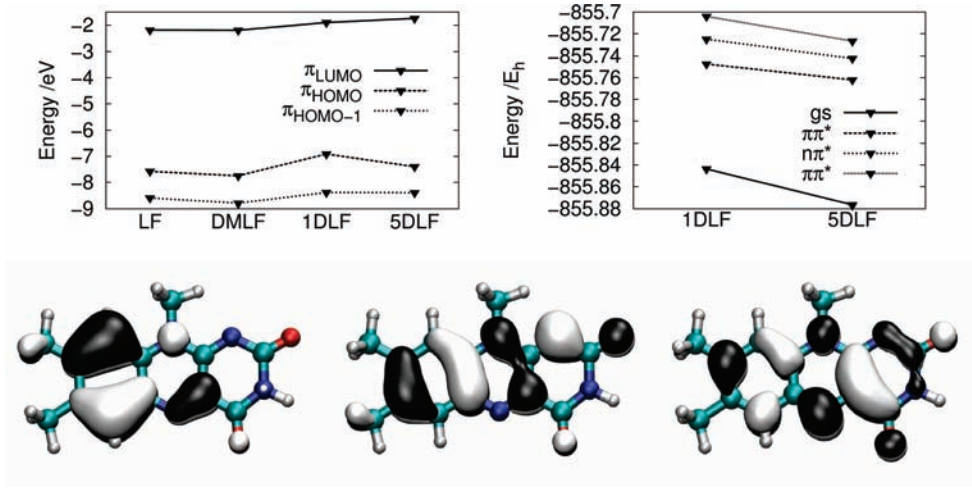

Figure 4. Left, top: Orbital energies of three frontier π orbitals for all calculated compounds in the vacuum. Right, top: Total energies of 1DLF in comparison to 5DLF. Bottom, left to right: π_{H-1} (HOMO-1), π_H (HOMO), and π_L* (LUMO) of LF. The black and white coding describes the different phases (plus or minus) of the molecular orbital amplitudes.

TABLE 3: Calculated Vertical Absorption Wavelengths, λ/nm, for LF and DMLF in Aqueous Solution Compared to Experimental Band Maxima for RF and DMRF[a]

	calculations (COSMO+μ-hyd.)			experiment	
state[b]	transition (LF)	λ LF	λ DMLF[c]	λ RF	λ DMRF
S_0	ground state				
S_1	$\pi_H \rightarrow \pi_L$*	432 (470)	421 (460)	450[d]	436[d]
S_4	$\pi_{H-1} \rightarrow \pi_L$*	357	344	375	349
S_3	$n_{N2} \rightarrow \pi_L$*	340	345		
	$n_{O2} \rightarrow \pi_L$*				
T_1	$\pi_H \rightarrow \pi_L$*	555	532		
T_3	$\pi_{H-1} \rightarrow \pi_L$*	455	445		
T_2	$n_{N2} \rightarrow \pi_L$*	377	382		
	$n_{O2} \rightarrow \pi_L$*				
	$n_{O1} \rightarrow \pi_L$*				

[a] The value of the calculated band maximum is given in parentheses. For more details, such as oscillator strengths and dipole moments, see the Supporting Information. [b] State ordering with respect to the vacuum calculation (see Supporting Information). [c] Vertical absorption energies taken from ref 9. [d] Absorption maxima in aqueous solution at ambient temperature taken from ref 22.

overlaps. The introduction of three methyl groups increases the number of normal modes by 27. Moreover, the torsional frequencies are very low. In combination with a large energy gap, the calculations become impracticable due to the immense number of vibrational levels in the final state. Rates for the ($S_1 \rightarrow T_1$) channel in LF were therefore evaluated employing a smaller integration interval and restrictions with respect to the excitation level of vibrational quanta (see Supporting Information for more information).

In order to estimate the ISC rate constants in water, the solvent shift of the electronic states has to be taken into account for the calculations of the SOME (derivatives) and the adiabatic electronic energy differences. Although with COSMO the charge distribution of the molecule that polarizes the surrounding solvent is taken into account properly only for the absorption energies, this is the only practicable way to introduce the solvent-induced shifts into the calculations of the SOME derivatives.

The COSMO model has been employed also for the calculations of adiabatic electronic energy differences (Table 6). Extensive tests (see Supporting Information, Table S13, Table S17, and Table S21) have shown that, by varying ΔE in a range of 1100 cm^{-1}, the order of magnitude of the ISC rate constant for the ($S_1 \rightarrow T_2$) channels remains stable. Our calculated ISC rate constants for vacuum and solution are found in Table 7.

LF and DMLF. We obtain a crossing between the S_1 and T_2 potential energy hypersurfaces along the reaction path connecting the FC region and the $^1(\pi\pi^*)$ minimum for LF and DMLF. This is the case both for vacuum and for aqueous solution. In the vacuum (Figure 5, left) the crossing is observed between the $^1(\pi\pi^*)$ (S_1) and the $^3(n\pi^*)$ (T_2) states. Spin−orbit coupling of the PEHs is substantial in that region. In agreement with El Sayed's rule, the direct ISC rate constants are found to be large (Table 7). Since the fastest process dominates the rate constant, we estimate that in the gas phase the ISC from the $S_1(\pi\pi^*)$ state to the triplet manifold takes place in nanoseconds for LF, and in about 100 ps for DMLF. This ISC channel is no longer available in aqueous solution, due to the significant blue shift of the $n\pi^*$ states. Instead, a crossing between the $^1(\pi\pi^*)$ (S_1) and the $^3(\pi\pi^*)$ (T_2) states takes place (Figure 5, right). However, spin−orbit matrix elements between the two states are negligible and, as a result, direct ISC is found to be very inefficient. Although this is in agreement with the widely used rules of thumb, it does not explain the substantial experimental ISC rate constants ($k_{ISC} = 10^8$ s^{-1}, ref 48) for RF in water. Only when vibronic spin−orbit coupling is taken into account, the rate constants reach values between $\sim 10^7$ and $\sim 10^8$ s^{-1} for the $S_1 \rightarrow T_{2x}$ and $S_1 \rightarrow T_{2y}$ channels of both compounds (Supporting Information, Tables S13 and S17). Qualitatively, this phenomenon can be interpreted as an intensity borrowing from the much faster $(\pi\pi^*) \rightarrow (n\pi^*)$ process.

1DLF and 5DLF. The DFT/MRCI energy profiles of 1DLF along the reaction path between the FC region and the $^1(\pi\pi^*)$ minimum are shown in Figure 6 (top). As already seen for the vertical excitation energies (FC region), there is no triplet state in close proximity to the first excited singlet state, independent of the environment. With the ISC initiating from the $^1(\pi\pi^*)$ (S_1) state, only the $^3(\pi\pi^*)$ (T_1) state can be populated. Vibronic spin−orbit coupling enhances the ISC rate constant to $\sim 10^5$ s^{-1} in the gas phase and $\sim 10^6$ s^{-1} in aqueous solution (see Supporting Information Table S19 for details). Nevertheless, ISC appears to be much too slow in 1DLF to be able to compete with IC or fluorescence decay.

No crossing between the S_1 and T_2 PEH is observed along the reaction path between the FC region and the $^1(\pi\pi^*)$

TABLE 4: Vertical Singlet and Triplet DFT/MRCI Excitation Wavelength, λ /nm, for 1DLF at the Ground State Geometry in the Vacuum and in Aqueous Solution[a]

	vacuum					COSMO + μ-hydr	experiment 1DRF
	state	transition	λ	$f(r)$	μ	λ	λ
S_0	$1^1A'$	ground state			9.1		
S_1	$2^1A'$	$\pi_H \rightarrow \pi_L^*$	473 (505)	0.276	11.3	515 (553)	537[b]
S_2	$1^1A'$	$n_O \rightarrow \pi_L^*$	374	0.001	3.6	320	
S_3	$2^1A''$	$n_{ON2} \rightarrow \pi_L^*$ $n_{ON1} \rightarrow \pi_L^*$	346	0.003	7.9	329	
S_4	$3^1A'$	$\pi_{H-1} \rightarrow \pi_L^*$	326	0.060	12.9	362	368
T_1	$1^3A'$	$\pi_H \rightarrow \pi_L^*$	660		9.6	693	
T_2	$2^3A'$	$n_O \rightarrow \pi_L^*$ $n_{ON2} \rightarrow \pi_L^*$	399		5.2	368	
T_3	$1^3A'$	$\pi_{H-1} \rightarrow \pi_L^*$ $\pi_H \rightarrow \pi_{L+1}^*$	399		12.3	447	

[a] The value in parentheses is the calculated band maximum. In addition to the dominant excitations, oscillator strengths $f(r)$ and dipole moments, μ/Debye, are given. For more details see the Supporting Information. Experimental values refer to 1DRF. [b] Absorption maxima in aqueous solution at ambient temperature taken from ref 22.

TABLE 5: Vertical Singlet and Triplet DFT/MRCI Excitation Wavelength, λ /nm, for 5DLF at the Ground State Geometry in Vacuum and Aqueous Solution[a]

	vacuum					COSMO + μ-hydr	experiment 5DRF
	state	transition	λ	$f(r)$	μ	λ	λ
S_0	$1^1A'$	ground state			9.8		
S_1	$2^1A'$	$\pi_H \rightarrow \pi_L^*$	397 (422)	0.324	9.5	385 (408)	400[b]
S_2	$1^1A'$	$n_{O2} \rightarrow \pi_L^*$	339	0.000	1.3		
S_3	$3^1A'$	$\pi_{H-1} \rightarrow \pi_L^*$ $\pi_H \rightarrow \pi_{L+1}^*$	304	0.151	13.2	325	335
T_1	$1^3A'$	$\pi_H \rightarrow \pi_L^*$	488		7.9	454	
T_2	$2^3A'$	$\pi_{H-1} \rightarrow \pi_L^*$	389		12.7	414	
T_3	$1^3A'$	$n_{O2} \rightarrow \pi_L^*$	347		1.7	320	

[a] The value in parentheses is the calculated band maximum. In addition to the dominant excitations, oscillator strengths $f(r)$ and dipole moments, μ/Debye, are given. For more details see the Supporting Information. Experimental values refer to 5DRF. [b] Absorption maxima in aqueous solution at ambient temperature taken from ref. [22]

TABLE 6: Adiabatic Excitation Wavelengths, λ/nm, and Radiative Rate Constants, k/s^{-1}, of the Lowest-Lying Singlet State[a]

	vacuum		exp
	$E_{adia}(S_1)$	k_F	k_F
LF[b]	456 (489)	6×10^7	5.6×10^7
DMLF[b]	461 (475)	5×10^7	3.8×10^7
1DLF	543 (556)	2×10^7	
5DLF	432 (449)	7×10^7	10×10^7

[a] ZPVE-corrected values are given in parentheses. The experimental fluorescence rates are obtained from τ_{Fl} and Φ_{Fl} (Table 1) via $k_F = \Phi_{Fl}/\tau_{Fl}$. [b] Excitation energies and fluorescence rate constants taken from ref 9.

TABLE 7: Integrated Rate Constants k_{ISC}/s^{-1} for the Intersystem Crossing from the Zero Vibrational Level of the First Electronically Excited Singlet State (S_1) to All Triplet Vibrational Levels (Electronic States T_1 and T_2) Located in a Small Energy Interval of Width 2η around the Initial State[a]

	vacuum		COSMO	
	k_{ISC} ($S_1 \rightarrow T_1$)	k_{ISC} ($S_1 \rightarrow T_2$)	k_{ISC} ($S_1 \rightarrow T_1$)	k_{ISC} ($S_1 \rightarrow T_2$)
LF	$\sim 10^5 - 10^6$	$\sim 10^9$	$\sim 3 \times 10^6$	$\sim 10^8$
DMLF	$\sim 1.6 \times 10^7$	$\sim 10^{10}$	$\sim 1 \times 10^7$	$\sim 10^7 - 10^8$
1DLF	$\sim 2 \times 10^6$		$\sim 1 \times 10^6$	
5DLF	$\sim 2 \times 10^6$		$\sim 7 \times 10^5$	$\sim 10^7 - 10^8$

[a] For detailed information on the procedure and the choice of parameters, see Supporting Information.

minimum for 5DLF in the isolated chromophore or in aqueous solution (Figure 6, bottom). In the vacuum, the minimum of the $^3(\pi\pi^*)$ T_2 state is situated closely above that of the S_1 state. With the ISC initiating from the $^1(\pi\pi^*)$ (S_1) state, only the $^3(\pi\pi^*)$ T_1 state can be populated. Vibronic spin−orbit coupling enhances the ISC rate constant to $\sim 10^5$ s^{-1}. In aqueous solution, however, the ordering of the $^1(\pi\pi^*)$ S_1 and the $^3(\pi\pi^*)$ T_2 states is altered. Although we do not observe a crossing between the $^1(\pi\pi^*)$ (S_1) and the $^3(\pi\pi^*)$ (T_2) states here, the minimum of the latter state should be energetically accessible from the initial state (S_1). When vibronic spin−orbit coupling is taken into account, our calculations predict the rate constant of ISC to range between $\sim 10^7$ and 10^8 s^{-1} for the $S_1 \rightarrow T_{2x}$ and $S_1 \rightarrow T_{2y}$ channels, respectively. For details see Supporting Information Table S22.

Depopulation of the $^1(\pi\pi^*)$ State. ***Processes in Water and Comparison with Experiment.*** Summarizing, the calculations yield fluorescence rates and ISC rates of comparable magnitude for LF. The phosphorescence rate (see Supporting Information) is significantly smaller. Hence, it is not necessary to take this process into consideration. These findings are in qualitative agreement with our experimental quantum yields Φ_F (0.27) and Φ_{Tr} (0.60) for RF. For a more quantitative comparison of the quantum yields, further processes such as the nonradiative depopulation of the S_1 state by internal conversion need to be taken into account. For the demethylated compounds (DMLF and DMRF, respectively), we find fluorescence rates of similar magnitude as for the parent compounds. However, our calculations cannot explain the significantly lower triplet quantum yield $\Phi_{Tr} = 0.23$ for DMRF. The fluorescence decay is found to be somewhat faster for 5DLF than for the parent compound.

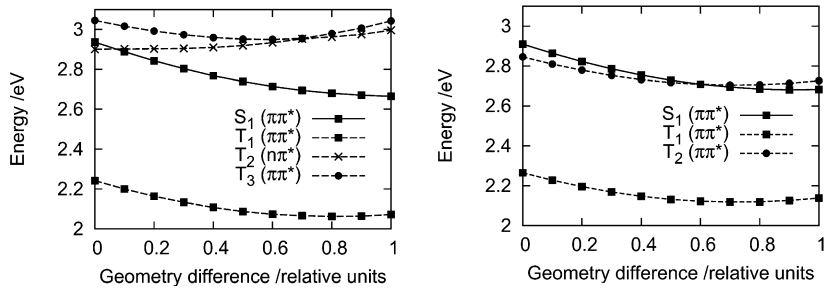

Figure 5. DFT/MRCI energies of low-lying states of LF along a linearly interpolated path between the ground state geometry (0) and the $^1(\pi\pi^*)$ geometry (1) for the vacuum (left) and aqueous solution (COSMO, right). For the energy profiles of DMLF, which are nearly identical, see ref.,[9] Figure 5.

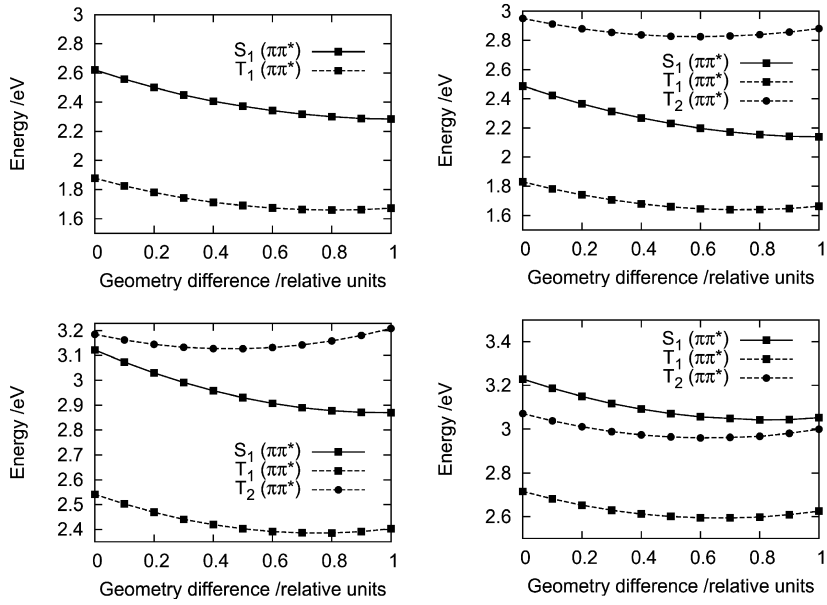

Figure 6. DFT/MRCI energies of low-lying states along a linearly interpolated path between the ground state geometry (0) and the $^1(\pi\pi^*)$ geometry (1) for 1DLF (top) and 5DLF (bottom) in the vacuum (left) and aqueous solution (COSMO, right).

Therefore, fluorescence should gain importance with respect to the ISC process, as is qualitatively reflected in the ratio of our experimental quantum yields Φ_F (0.52) and Φ_{Tr} (0.64). These values add up to more than 1.0, but errors between 10 and 15% should be considered. In 1DRF, an ultrafast fluorescence decay was observed.[34] The mechanism of the quenching process is not known at present and needs further clarification.

Processes in the Gas Phase. For LF and DMLF, our calculations find the nonradiative depletion more than 1 order of magnitude faster than the spin-allowed radiative transition to the electronic ground state. Our results suggest that internal conversion to the ground state enhanced by the energetic proximity of the first $^1(n\pi^*)$ state is an additional competing channel. On this basis, we predict that for isolated LF (RF) and DMLF (DMRF) fluorescence should not be observable. Because of the lack of a second accessible triplet state, the ISC rate in excited 5DLF is found to be more than 1 order of magnitude smaller than in the parent compound. Furthermore, $^1(n\pi^*)$ states should not participate actively in the nonradiative decay of the S_1 state. Accordingly, deactivation via fluorescence should prevail for 5DLF (5DRF) in the gas phase. ISC cannot compete with the spin-allowed radiative transition to the electronic ground state in excited 1DLF. Additionally, $^1(n\pi^*)$ states are not accessible. Thus, triplet generation in 1DLF should be negligible and radiative decay via fluorescence should be substantial.

Triplet−Triplet Absorption. It has been found earlier that triplet−triplet absorption spectra of LF calculated in the gas phase cannot be compared to measurements in aqueous solution.[14] Since the triplet−triplet excitation energies significantly depend on the surrounding environment, we employ our full solvent model (COSMO + μ-hydr), although, as described above, the treatment of solvent effects with COSMO for non-FC excitations is not ideal. The resulting line spectra of the vertical triplet−triplet excitation energies are displayed and compared to our experimental data in Figure 7.

When we compare the calculated line spectra with our experimental data, we have to keep in mind that the reciprocal wavelength scale is very sensitive in the low energy regime. The typical DFT/MRCI error bars of ±0.2 eV[49] translate to ±20 nm (around 360 nm) up to ±90 nm (around 700 nm). The majority of the excited triplet states show substantial multiconfiguration character. However, we could find three different electronic transitions (labeled A, C, D in the following, see Table 8) for all investigated flavins that contribute with significant intensity to the transient spectra. In addition, two different electronic excitations (labeled B, see Table 8) with minor intensity are found.

We find four $T_1 \rightarrow T_n$ excitations with substantial oscillator strength for the parent compound (LF) within the detection range of the experiment. The lowest-lying transition with high intensity is dominated by the ($\pi_{H-3} \rightarrow \pi_H$) excitation (A-type) and is assigned to the experimental maximum at 700 nm (see Table 2). In good agreement with the experiment, this transition shows the highest oscillator strength in the detection range. The second

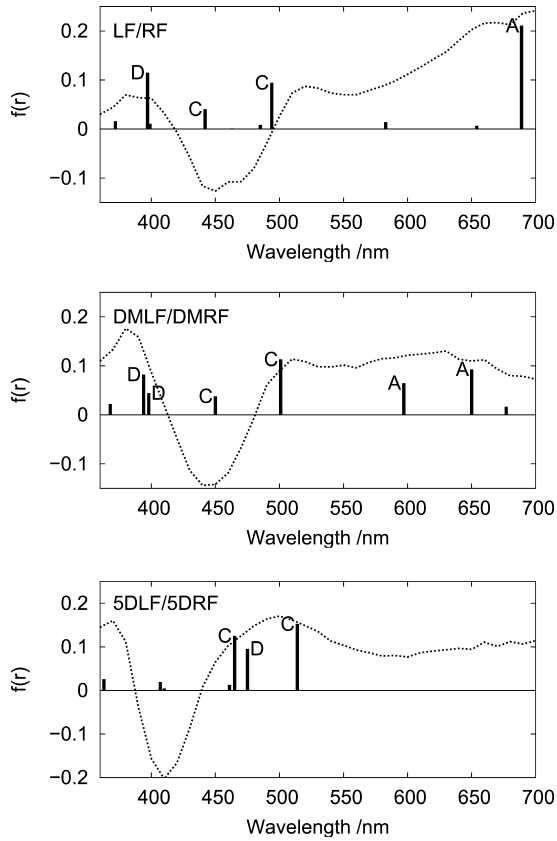

Figure 7. Comparison of the experimental and calculated (COSMO + μ-hydr) triplet−triplet absorption spectra of the parent compound and the demethyl and 5-deaza derivatives. Only states with an oscillator strength $f(r) > 0.01$ are shown. For the definition of the labels A, C, and D, see Table 8.

TABLE 8: LF. Assignment of the Vertical Triplet−Triplet Excitation Wavelengths λ /nm to the Electronic Structure[a]

transitions		λ			
label	excitation	LF	DMLF	1DLF	5DLF
A	$\pi_{H-3}\rightarrow\pi_H$	689 (vs)	650, 597 (s), (s)	690, 601 (s), (s)	752 (s)
B[b]	$\pi_{H-2}\rightarrow\pi_H$	583 (w)	677 (w)	506 (m[c])	879 (w)
	$\pi_L\rightarrow\pi_{L+1}$*				
C	$\pi_{H-4}\rightarrow\pi_H$	494, 442 (s), (m)	501, 450 (s), (m)	448 (s)	514, 465 (vs), (s)
	$\pi_L\rightarrow\pi_{L+2}$*				
D	$\pi_L\rightarrow\pi_{L+3}$*	397 (s)	398, 394 (m), (s)	397 (vs)	475 (s)

[a] The electronic excitations are given with respect to the open-shell triplet ground state. Intensities are indicated in parentheses. [b] Electronic excitations under "B" are of lower intensity and are not shown in Figure 7. [c] Small contributions of C-type and D-Type configuration increase the intensity.

and third optically bright states are attributed to linear combinations of the ($\pi_{H-4}\rightarrow\pi_H$) and ($\pi_L\rightarrow\pi_{L+2}$) configurations (C-type) with minor contributions of double excitations. The lower-lying states are assigned to the experimental maximum at 520 nm. Unfortunately, this transition is partially overlaid by the absorbance minimum caused by the bleaching. Its oscillator strength is roughly half of that of the A-type transition. This is reflected by the experiment. The higher-lying C-type state is completely obscured by the absorbance minimum. In fact, it was shown by Swartz et al.[50] that the triplet absorption of FMN in water solution in this spectral region is only slightly less intense than at 600−700 nm, supporting our theoretical findings. The fourth bright state is dominated by the ($\pi_L\rightarrow\pi_{L+3}$) excitation (D-type). Its transition wavelength compares well with the maximum around 390 nm in our experiment. A linear combination of the ($\pi_{H-2}\rightarrow\pi_H$) and ($\pi_L\rightarrow\pi_{L+1}$) configurations (b-type) is found in between the A-type and the low-lying C-type state. This dark state is isolated from the optically bright in LF, whereas this order changes in the other compounds.

The absorption spectrum of DMLF/DMRF is different from that of the parent compound. The lowest-lying maximum (630 nm) of the transient spectrum exhibits reduced intensity and a blue shift. Two excited states with substantial oscillator strength are found in this wavelength region. They arise from linear combinations of A-type and b-type electronic states causing a distribution of the A-type transition probability among two bands. Inspection of the shape of the π_{H-3} MO gives an explanation for the blue shift of the A-type states. This particular MO shows substantial electron density at the C(7)−C(8) bond. Apparently, the removal of methyl groups from the two carbon atoms C7 and C8 strengthens this bond. Hence, the π_{H-3} MO is stabilized and promotion of one electron out of this MO is energetically less favorable. The energetic locations and intensities of the C-type peaks in DMLF and LF are similar. The longer wavelength transition can be assigned to the transient absorption maximum at 510 nm, whereas the other one is found again in the region of the bleach peak. Linear combination with double excitations causes the D-type configuration to distribute the intensity among two nearly degenerated transitions. Similar to the corresponding parent compound these transitions contribute to the shortest wavelength maximum in the observation range.

The excited state with A-type electronic structure is red shifted in 5DLF with respect to the parent compound. Our calculations predict the transition to be located at 752 nm, which is outside the experimental detection range. Admixture with b-type configurations does not occur in this compound because of a substantial red shift of the corresponding transition (see Table 8). Close to the experimental maximum, at 500 nm, three excited states with C- and D-type structure are found that all contribute intensity in that spectral region.

Conclusion

Structural and electronic changes that were introduced into riboflavin by chemical synthesis (the 1- and 5-deaza-derivatives and the 7,8-didemethyl and 8-isopropyl riboflavins) cause significant changes in the photophysical and photochemical properties of these compounds. In particular, the deaza compounds exhibit strongly changed absorbances (a hypsochromic shift for 5DRF and a bathochromic absorption for 1DRF). They also have different fluorescence properties; no steady state fluorescence could be measured for 1DRF (and only ultrafast measurements revealed a fluorescence for this compound), whereas 5DRF showed a significantly enhanced fluorescence yield. Also the triplet formation and decay processes are different from those of the parent RF. The DMRF derivative showed a much smaller triplet yield, whereas the triplet yields of *ipr*RF and RF were quite similar. The most interesting result is surely the absence of a triplet formation pathway for 1DRF, a finding that is excellently explained by the calculations.

The absorption properties of the parent compound and the derivatives are reflected in a convincing manner by our quantum chemical calculations on the lumiflavins. The results show that two aspects should be considered when the calculated values are compared to the experimental band maxima of the com-

pounds in solution. First, the vertical excitation energy is blue shifted with respect to the band maximum and second, solvent shifts play a decisive role in the energetic position of the absorption bands of the two deaza compounds. With our best solvent model (COSMO and μ-hydration with four water molecules), the calculated absorption maxima fit remarkably well the experimental values.

We predict that fast (spin-forbidden) nonradiative processes quench the fluorescence of excited LF and DMLF in the gas phase. Our calculations show that ISC cannot compete with deactivation via fluorescence in 1DLF and 5DLF. Whereas we expect substantial fluorescence from excited 5DLF, we cannot exclude the involvement of ultrafast spin-allowed nonradiative processes in 1DLF.

Intersystem crossing takes place from the S_1 $^1(\pi\pi^*)$ to the T_2 $^3(\pi\pi^*)$ state by a vibronic spin−orbit coupling mechanism in aqueous solutions of RF, DMRF, *ipr*RF, and 5DRF. The rate for triplet formation from the S_1 state is small in excited 1DLF due to the absence of a close-by triplet state. Accordingly, no triplet state formation is observed for that riboflavin derivative.

Abbreviations

1DLF, 1-deazalumiflavin; 1DRF, 1-deazariboflavin; 5DLF, 5- deazalumiflavin; 5DRF, 5-deazariboflavin; COSMO, conductor-like screening model; DFT, density functional theory; DFT/MRCI, density functional theory/ multireference configuration interaction; DMLF, 7,8-didemethyllumiflavin = 10-methylisoalloxazine; DMRF, 7,8-didemethyl riboflavin; FAD, flavin adenine dinucleotide; FC, Franck−Condon; FMN, flavin mononucleotide; fwhm, full width at half-maximum; IA, isoalloxazine; *ipr*RF, 8-isopropylriboflavin; ISC, intersystem crossing; LF, lumiflavin; MRSOCI, multireference spin−orbit coupling configuration interaction; PEH, potential energy hypersurface; RF, riboflavin; SOMES, spin−orbit matrix elements; SPOCK, spin−orbit coupling kit; TDDFT, time-dependent density functional theory; TZVP, valence triple-ζ with (1d/1p) polarization; UDFT, unrestricted density functional theory: ZPVE, zero-point vibrational energy.

Acknowledgment. This work has been performed as a project of the SFB663 (B3 and C1) at the Heinrich-Heine University Düsseldorf and is printed at its instigation with financial support provided by the Deutsche Forschungsgemeinschaft. We thank the referees for valuable comments.

Supporting Information Available: Molecular orbitals and vertical excitation energies in vacuum and different solvent models and a comparison of the geometries of the ground and the $^1(\pi\pi^*)$ states is included. In addition, a comparison of the vibronic absorption spectra (calculated and measured) is given, as well as the radiative fluorescence and phosphorescence rate constants. A detailed set of calculations for the intersystem crossing rates, as well as the relevant literature for these chapters. This material is available free of charge via the Internet at http://pubs.acs.org.

References and Notes

(1) Silva, E., Edwards, A. M., Eds.; *Flavins Photochemistry and Photobiology*; RSC Publishing: Cambridge, England, 2006.

(2) Briggs, W. R.; Christie, J. M. *Trends Plant Sc.* **2002**, *7*, 204–210.

(3) Losi, A. Flavin-based photoreceptors in bacteria. In *Flavin photochemistry and photobiology*, IV ed.; Silva, E., Edwards, A. M., Eds.; Elsevier: Amsterdam, The Netherlands, 2006; pp 223−269.

(4) Losi, A. *Photochem. Photobiol.* **2007**, *83*, 1283–1300.

(5) Edmondson, D. E.; Ghisla, S. Flavoenzyme Structure and Function. In *Methods in Molecular Biology*; Chapman, S. K., Reid G. A., Eds.; Humana Press Inc.: Totowa, NJ, 1999; vol. 131, pp 157−179.

(6) Scola-Nagelschneider, G.; Hemmerich, P. *Eur. J. Biochem.* **1976**, *66*, 567–577.

(7) Kasai, S.; Fritz, B. J.; Matsui, K. *Bull. Chem. Soc. Jpn.* **1987**, *60*, 3041–3042.

(8) Murthy, Y. V. S. N.; Massey, V. *J. Biol. Chem.* **1998**, *273*, 8975–8982.

(9) Salzmann, S.; Tatchen, J.; Marian, C. M. *J. Photochem. Photobiol., A* **2008**, *198*, 221–231.

(10) Hasegawa, J.; Bureekaew, S.; Nakatsuji, H. *J. Photochem. Photobiol., A* **2007**, *189*, 205–210.

(11) Climent, T.; González, R.; Merchán, M.; Serrano-Andrés, L. *J. Phys. Chem. A* **2006**, *110*, 13584–13590.

(12) Sikorska, E.; Khmelinskii, I. V.; Koput, J.; Bourdelande, J. L.; Sikorski, M. *J. Mol. Struct.* **2004**, *697*, 137–141.

(13) Sikorska, E.; Khmelinskii, I. V.; Worrall, D. R.; Koput, J.; Sikorski, M. *J. Fluoresc.* **2004**, *14*, 57–64.

(14) Neiss, C.; Saalfrank, P.; Parac, M.; Grimme, S. *J. Phys. Chem. A* **2003**, *107*, 140–147.

(15) Zenichowski, K.; Gothe, M.; Saalfrank, P. *J. Photochem. Photobiol., A* **2007**, *190*, 290–300.

(16) Domratcheva, T.; Fedorov, R.; Schlichting, I. *J. Chem. Theory Comput.* **2006**, *2*, 1565–1574.

(17) Dittrich, M.; Freddolino, P. L.; Schulten, K. *J. Phys. Chem. B* **2005**, *109*, 13006–13013.

(18) Domratcheva, T.; Grigorenko, B. L.; Schlichting, I.; Nemukhin, A. V. *Biophys. J.* **2008**, *94*, 3872–3879.

(19) Götze, J.; Saalfrank, P. *J. Photochem. Photobiol., B* **2009**, *94*, 87–95.

(20) Sadeghian, K.; Bocola, M.; Schütz, M. *J. Am. Chem. Soc.* **2008**, *130*, 12501–12513.

(21) Silva-Junior, M. R.; Salzmann, S., Marian, C. M., Thiel, W. **2009**, submitted to *J. Phy. Chem.*

(22) Mansurova, M.; Koay, M. S.; Gärtner, W. *Eur. J. Org. Chem.* **2008**, 5401–5406.

(23) Kleinschmidt, M.; Tatchen, J.; Marian, C. M. *J. Chem. Phys.* **2006**, *124*, 124101.

(24) Tatchen, J. *VIBES*; Universität Düsseldorf: Düsseldorf, Germany, 2005.

(25) Kleinschmidt, M.; Tatchen, J.; Marian, C. M. *J. Comput. Chem.* **2002**, *23*, 824–833.

(26) Kleinschmidt, M.; Marian, C. M. *Chem. Phys.* **2005**, *311*, 71–79.

(27) Hess, B. A.; Marian, C. M.; Wahlgren, U.; Gropen, O. *Chem. Phys. Lett.* **1996**, *251*, 365–371.

(28) Schimmelpfennig, B. *AMFI*; Stockholm University: Stockholm, Sweden, 1996.

(29) Tatchen, J.; Marian, C. M. *Chem. Phys. Lett.* **1999**, *313*, 351–357.

(30) Danovich, D.; Marian, C. M.; Neuheuser, T.; Peyerimhoff, S. D.; Shaik, S. *J. Phys. Chem. A* **1998**, *102*, 5923–5936.

(31) Tatchen, J.; Gilka, N.; Marian, C. M. *Phys. Chem. Chem. Phys.* **2007**, *9*, 5209–5221.

(32) Ahlrichs, R.; Bär, M.; Baron, H.-P.; Bauernschmitt, R.; Böcker, S.; Crawford, N.; Deglmann, P.; Ehrig, M.; Eichkorn, K.; Elliott, S.; Furche, F.; Haase, F.; Häser, M.; Hättig, C.; Hellweg, A.; Horn, H.; Huber, C.; Huniar, U.; Kattannek, M.; Köhn, A.; Kölmel, C.; Kollwitz, M.; May, K.; Nava, P.; Ochsenfeld, C.; Öhm, H.; Patzelt, H.; Rappoport, D.; Rubner, O.; Schäfer, A.; Schneider, U.; Sierka, M.; Treutler, O.; Unterreiner, B.; von Arnim, M.; Weigend, F.; Weis, P.; Weiss, H.; *TURBOMOLE V510*; University of Karlsruhe: Karlsruhe, Germany, 2008.

(33) Spencer, R.; Fisher, J.; Walsh, C. *Biochemistry* **1977**, *16*, 3586–3594.

(34) Slavov, C.; Mansurova, M.; Holzwarth, A. R.; Gärtner, W. *Photochem. Photobiol.*, submitted for publication.

(35) Drössler, P.; Holzer, W.; Penzkofer, A.; Hegemann, P. *Chem. Phys.* **2003**, *286*, 409–420.

(36) Insińska-Rak, M.; Sikorska, E.; Bourdelande, J. L.; Khmelinskii, I. V.; Prukała, W.; Dobek, K.; Karolczak, J.; Machado, I. F.; Ferreira, L. F. V.; Komasa, A.; Worrall, D. R.; Sikorski, M. *J. Mol. Struct.* **2006**, *783*, 184–190.

(37) Crovetto, L.; Martinez-Junza, V.; Braslavsky, S. E. *Photochem. Photobiol.* **2006**, *82*, 281–290.

(38) Chacon, J. N.; McLearie, J.; Sinclair, R. S. *Photochem. Photobiol.* **1988**, *47*, 647–656.

(39) Grodowski, M. S.; Veyret, B.; Weiss, K. *Photochem. Photobiol.* **1977**, *26*, 341–352.

(40) Dudley, K. H.; Ehrenberg, A.; Hemmerich, P.; Müller, F. *Helv. Chim. Acta* **1964**, *47*, 1354–1383.

(41) Sung, M.; Moore, T. A.; Song, P.-S. *J. Am. Chem. Soc.* **1972**, *94*, 1730–1740.

(42) Bowd, A.; Byrom, P.; Hudson, J. B.; Turnbull, J. H. *Photochem. Photobiol.* **1968**, *8*, 1–10.
(43) Visser, A. J. W. G.; Müller, F. *Helv. Chim. Acta* **1979**, *62*, 593–608.
(44) Bomble, Y. J.; Sattelmeyer, K. W.; Stanton, J. F.; Gauss, J. *J. Chem. Phys.* **2004**, *121*, 5236–5240.
(45) Davidson, E. R.; Jarzęcki. A, *Chem. Phys. Lett.* **1998**, *285*, 155–159.
(46) Cederbaum, L. S.; Domcke, W. *J. Chem. Phys.* **1976**, *64*, 603–611.
(47) Weigel, A.; Dobryakov, A. L.; Veiga, M.; Pèrez Lustres, J. L. *J. Phys. Chem. A* **2008**, *112*, 1205412065) .
(48) Kennis, J. T. M.; Crosson, S.; Gauden, M.; van Stokkum, I. H. M.; Moffat, K.; van Grondelle, R. *Biochemistry* **2003**, *42*, 3385–3392.
(49) Silva-Junior, M. R.; Schreiber, M.; Thiel, W. *J. Chem. Phys.* **2008**, *129*, 1–14.
(50) Swartz, T. E.; Carchnoy, S. B.; Christie, J. M.; Lewis, J. W.; Szundi, I.; Briggs, W. R.; Bogomolni, R. A. *J. Biol. Chem.* **2001**, *276*, 36493–36500.

JP905724B